Hierarchical Self-assembly and Controlled Disassembly of a Cavitand-based Host-Guest Supramolecular Polymer

Polymer Chemistry

ROYAL SOCIETY OF CHEMISTRY

PAPER

View Article Online
View Journal

Cite this: DOI: 10.1039/d0py01483d

Hierarchical self-assembly and controlled disassembly of a cavitand-based host–guest supramolecular polymer†

Daniele Zuccaccia,[a] Roberta Pinalli,[b] Rita De Zorzi,[c] Monica Semeraro,[d] Alberto Credi,*[d] Cristiano Zuccaccia,[e] Alceo Macchioni,[e] Silvano Geremia*[c] and Enrico Dalcanale*[b]

There is considerable interest in dynamic materials featuring modular components with nano-scale dimensions and controlled responsiveness to external stimuli. Supramolecular polymers are a class of materials that fulfil all these conditions well. Here, we present a family of host–guest supramolecular polymers that combine the outstanding complexing properties of tetraphosphonate cavitands toward *N*-methylpyridinium guests with molecular switching. The designed monomer is a cavitand featuring four inward facing P═O groups at the upper rim and a single *N*-methylpyridinium unit at the lower rim, forming instantaneously a polymeric species in solution, thanks to the high complexation constants measured for these host–guest interactions. This system has been analyzed by NMR spectroscopy and electrochemical techniques. In order to interpret the results of diffusion-sensitive experiments, we took advantage of the X-ray crystal structure obtained for the polymeric species and developed an original treatment for the PGSE data by non-linear fitting. The analysis of the experimental data identified an isodesmic polymerization model at a monomer concentration below 20 mM, driven by intrachain host–guest interactions, and an additional level of tetrameric bundle aggregation above 20 mM, due to interchain dipolar and quadrupolar interactions. Two orthogonal disassembly procedures have been implemented: electrochemical reduction for the linear chains and solvent-driven dissolution for the bundles.

Received 21st October 2020,
Accepted 26th November 2020

DOI: 10.1039/d0py01483d

rsc.li/polymers

Introduction

Dynamic polymers (DYNAMERS) are drawing the attention of the material scientists community since they display specific responsiveness to external stimuli, adaptation to environmental changes and self-healing capability.[1,2] Supramolecular polymers, held together by non-covalent interactions, are a class of materials that fulfil all these conditions well.[3] The basic idea of supramolecular polymers derives directly from the observation of the biological fibrous architectures in the extracellular matrix such as the cell cytoskeleton.[3] Biological systems evolved towards non-covalent polymers due to their flexibility and ability to respond efficiently and in a timely manner to external stimuli, essential requirements to survive in changing environments.[4] Synthetic supramolecular polymers that mimic the properties of biological systems are exploited in a wide range of technological applications, from biomedical and biomimetic devices[5,6] to photovoltaic and semiconducting materials.[7]

Different approaches have been applied in the design of the building blocks of supramolecular polymers, starting from the first examples of systems based on hydrogen bonding[8] or on metal coordination,[9] followed by self-assembled supramolecular polymers fully or partially created from an orthogonal combination of multiple non-covalent binding interactions.[10] A general strategy takes advantage of synergistic interactions with a fast kinetic profile and a behaviour controlled by the thermodynamic constants. In fact, unlikely the covalent polymers that generally display a kinetically controlled behaviour,

[a]*Dipartimento di Scienze Agroalimentari Ambientali e Animali, Università di Udine, Via Cotonificio 108, 33100 Udine, Italy*
[b]*Dipartimento di Scienze Chimiche, della Vita e della Sostenibilità Ambientale and Unità INSTM, UdR Parma, Università di Parma, Viale delle Scienze 17/A, 43124 Parma, Italy. E-mail: enrico.dalcanale@unipr.it*
[c]*Dipartimento di Scienze Chimiche e Farmaceutiche, Università di Trieste, via Giorgieri 1, 34127 Trieste, Italy. E-mail: sgeremia@units.it*
[d]*Dipartimento di Chimica Industriale "Toso Montanari", Università di Bologna, Viale del Risorgimento 4, 40136 Bologna, Italy. E-mail: alberto.credi@unibo.it*
[e]*Dipartimento Chimica, Biologia e Biotecnologia and CIRCC, Università di Perugia, Via Elce di Sotto 8, 06123 Perugia, Italy*

† Electronic supplementary information (ESI) available: Calculation of the hydrodynamic translational diffusion coefficients; SEK model; AK model; SEK-TA*i* model; SEK-TAi[4] model; Fig. S1–S13 NMR studies; Fig. S14–S15 cyclic voltammograms; Table S1 thermodynamic constants; Table S2 average degree of polymerization calculated with different models. See DOI: 10.1039/d0py01483d

in supramolecular polymers, thermodynamics plays a pivotal role in the association of the building blocks and in the behaviour of the stimuli-responsive polymer.

Recently, new studies on supramolecular polymers have started to exploit host–guest interactions designing systems with cyclodextrins,[11] cucurbiturils,[12] pillararenes,[13] calixarenes[14,15] and cavitands[16–18] as receptors. Among these, systems based on tetraphosphonate cavitands with their all-inward configuration and ammonium salts proved to be suitable monomers for new supramolecular polymers[19,20] and for polymer blending[21,22] because of their outstanding complexation properties and high association constants. Previously, we reported the formation in solution and in the solid state of a supramolecular polymer with ditopic building blocks, having a phosphonate cavitand as the host functionality and an *N*-methylpyridinium moiety bound to the lower rim of the cavitand as the guest functionality.[19] In solution this monomer forms instantaneously a polymer, thanks to the high complexation constants ($K_a \approx 10^7$ M^{-1}) measured for these host–guest interactions and the responsiveness of these polymers to external stimuli has been verified by the addition of a competitive guest (*N*-butylmethylammonium iodide salt, $K_a \approx 10^{10}$ M^{-1}) for dissociation, followed by base-driven reassembly.[19]

Electrochemical experiments on model systems have shown that one-electron reduction of the *N*-methylpyridinium guests leads to decomplexation.[23] Since the monoelectronic reduction of the investigated guests is reversible, it may be envisaged that the formation and dissociation of such complexes can be electrochemically controlled.

In this work, we demonstrate that the assembly of high molecular weight host–guest polymers proceeds through the formation of bundles. The aggregation modes of this class of supramolecular polymers are revealed by a variety of spectroscopic and electrochemical measurements, supported by theoretical polymerization models. Bundle formation is triggered by a concentration threshold above which the aggregation of oligomeric chains is favoured over the isodesmic growth of a single chain. The difference in the nature of the weak interactions involved in the two assembly modes allows implementing orthogonal disassembly procedures in the form of electrochemical reduction for the linear chains and solvent-driven dissolution for the bundles.

Experimental

NMR spectroscopy

One-dimensional ^{1}H, ^{13}C, ^{19}F and ^{31}P NMR spectra were measured on Bruker DRX 400 spectrometers equipped with a GREAT 1/10 gradient unit and a QNP probe with a *Z*-gradient coil. Referencing is relative to TMS (^{1}H and ^{13}C), CCl_3F (^{19}F), and 85% H_3PO_4 (^{31}P). NMR samples were prepared by dissolving a suitable amount of compound in 0.5 mL of the appropriate solvent. All measurements were performed at 296 K, unless otherwise stated.

Two-dimensional ^{1}H-NOESY and ^{1}H-EXSY[24] NMR experimental results were acquired by the standard three-pulse sequence or by the PFG version.[25] Two-dimensional ^{19}F, ^{1}H-HOESY NMR experimental results were acquired using the standard four-pulse sequence or the modified version.[26] The number of transients and the number of data points were chosen according to the sample concentration and to the desired final digital resolution. Semi-quantitative ^{1}H-NOESY and ^{19}F and ^{1}H-HOESY NMR spectra were acquired using a 2 s relaxation delay and 800 ms mixing times.

Quantitative ^{1}H-EXSY NMR experiments were carried out with a relaxation delay of 5 s and a mixing time (τ_m) ranging from 0.01 s to 0.3 s. For an uncoupled system of spins undergoing chemical exchange between sites A and B, with the simplification of equal spin–lattice relaxation time, the exchange rate constants (k_{obs}) between site A and site B can be estimated using eqn (1) and (2)

$$\ln\left(\frac{r+1}{r-1}\right) = k_{obs}\tau_m \quad (1)$$

$$r = \frac{4X_aX_b(I_{aa}+I_{bb})}{(I_{ab}+I_{ba})} - (X_a - X_b) \quad (2)$$

where I_{aa}, I_{bb}, I_{ab} and I_{ba} represent diagonal- and cross-peak volumes, respectively, and X_a and X_b the molar fractions of species A and B.[27] In the present case, A and B denote free tetraphosphonate cavitand and tetraphosphonate cavitand with encapsulated *N*-methyl-pyridinium. The diagonal- and cross-peak volumes were measured using "XWinNMR" Bruker software after phase and baseline corrections in both dimensions. The volume uncertainty was estimated by determining the volume of the noise signal in a 'blank region' of the 2D-spectra. Molar fractions X_a and X_b were obtained from the integration of the corresponding ^{1}H NMR spectrum. Linear regressions of experimental values using eqn (1) to estimate k_{obs} were performed by means of the software package Microcal Origin 7.0.

PGSE measurements

PGSE NMR measurements were performed by using the standard stimulated echo pulse sequence[28] without spinning.

The dependence of the resonance intensity (I) on a constant waiting time and on a varied gradient strength (G) is described by eqn (3):

$$I = I_0 \exp\left[-(\gamma\delta)^2 D_t\left(\Delta - \frac{\delta}{3}\right)G^2\right] \quad (3)$$

where I is the intensity of the observed spin echo, I_0 is the intensity of the spin echo without gradients, D_t is the translational diffusion coefficient, Δ is the delay between the midpoints of the gradients, δ is the length of the gradient pulse, and γ is the magnetogyric ratio. The shape of the gradients was rectangular, their duration (δ) was 5 ms, and their strength (G) varied during the experiments. Different values of Δ (120, 300, 600, 1800 ms), "nt" (number of transients) and number of different gradient strengths (G) were used for different

samples. In the case of a single species or a monodisperse distribution of species in fast exchange in the diffusion NMR timescale (Δ), D_t can be obtained from the linear regression of the semi-logarithmic plots of $\ln(I/I_0)$ *vs.* G^2 by measuring the instrumental constant, using a sample of HDO (5%) in D_2O (known diffusion coefficient in the range 274–318 K)[29,30] under the same exact condition as the sample of interest. Temperature and gradient pulse fluctuations as well as variation of fluid viscosity (η) with increasing sample concentration were taken into account using tetrakis-(trimethylsilyl) silane (TMSS) as the internal standard. D_t data were treated as described in the literature.[28] The measurement uncertainty was estimated to be approximately 3–4% in D_t.

Fitting

Evaluation of the translational diffusion coefficients, calculation of the distribution of polymeric species and fitting of the experimental PGSE data to optimize the polymerization parameters have been performed using the software Octave[31] and, in particular, the package Optim. Scripts developed for this analysis are deposited in the ESI.†

Electrochemical experiments

Cyclic voltammetry (CV) and differential pulse voltammetry (DPV) experiments were carried out in argon-purged CH_2Cl_2 (Romil Hi-Dry) at room temperature with an Autolab 30 multipurpose instrument interfaced to a PC. The working electrode was a glassy carbon electrode (Amel; 0.07 cm^2), the counter electrode was a Pt wire, separated from the solution by a frit, and an Ag wire was employed as a quasi-reference electrode. Ferrocene was used as an internal standard ($E_{1/2}$ = +0.46 V *vs.* SCE). Tetrabutylammonium hexafluorophosphate was employed as the supporting electrolyte, and the examined potential window ranged between −2.0 V and +2.0 V *vs.* SCE. The IR compensation implemented within the Autolab 30 was used, and every effort was made throughout the experiments to minimise the resistance of the solution. In any instance, the full electrochemical reversibility of the voltammetric wave of ferrocene was taken as an indicator of the absence of uncompensated resistance effects. For reversible processes, the half-wave potential values were calculated from an average of CV and DPV experiments, whereas the redox potential values in the case of irreversible processes were estimated from the DPV peaks. Experimental errors: potential values, 10 mV for reversible processes, 20 mV for irreversible processes. Spectroelectrochemical measurements were performed *in situ* with a custom-made optically transparent thin-layer electrochemical (OTTLE) cell by using an Autolab 30 potentiostat and an Agilent Technologies 8543 diode array spectrophotometer. The working and counter electrodes were Pt minigrids, and the quasi-reference electrode was an Ag wire; all the electrodes were melt-sealed into a polyethylene spacer. The thickness of the layer, determined by spectrophotometry, was about 180 μm.

Results and discussion

The family of host–guest supramolecular polymers formed by ditopic building blocks, having a phosphonate cavitand as the host functionality and an *N*-methylpyridinium moiety bound to the lower rim of the cavitand as the guest functionality, has been designed, prepared and characterized previously.[19] The crystal structure (Fig. 1) of the homopolymer **1I** (Scheme 1) gives evidence of the two major interactions responsible for the complexation: multiple ion–dipole interactions between the inward-facing P═O groups and the positively charged methylpyridinium moiety, and directional hydrogen bonds involving the acidic methyl group with the π-basic cavity (cation–π interaction) and the *ortho* H-pyridinium atoms with two opposite P═O groups. The crystal packing (Fig. 1) shows that each linear polymeric chain packs against other four antiparallel chains. Furthermore, in the crystallographic structure, the counterions are located in between the lower rim and the alkyl chains, close to the methylpyridinium fragment. The characterization in solution performed by ITC (Isothermal Titration Calorimetry) on **2·3PF$_6$** (a suitable model of a single monomer–monomer connection) indicates a high association constant ranging from 10^4 in MeOH to 10^7 M^{-1} in dichloromethane. Finally, by static light scattering in a batch off-line model the weight-averaged molecular weight of the polymer was determined only at medium-low concentration values (below 20 mM) indicating a degree of polymerization of about 18 units.[19]

The aim of this study is to deepen our understanding about the solution behaviour of this class of ionic supramolecular

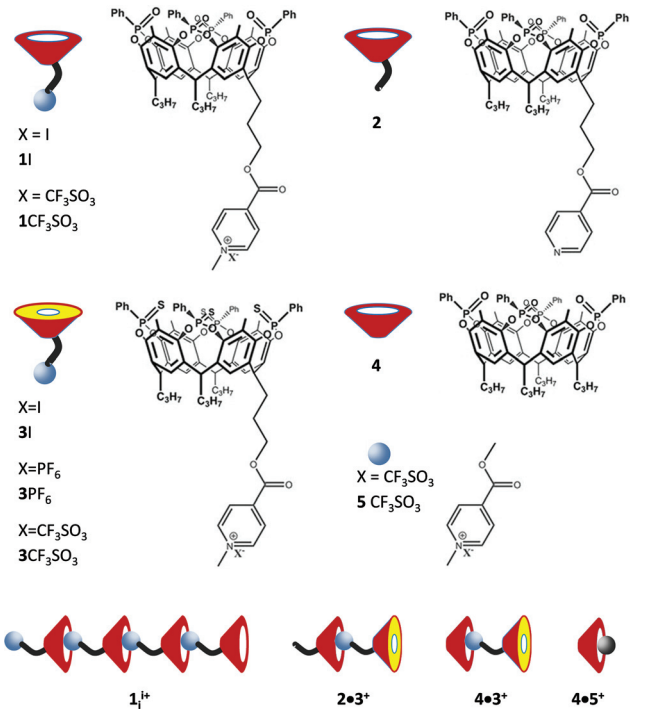

Scheme 1 The ionic host–guest cavitands investigated by electrochemical and NMR experiments.

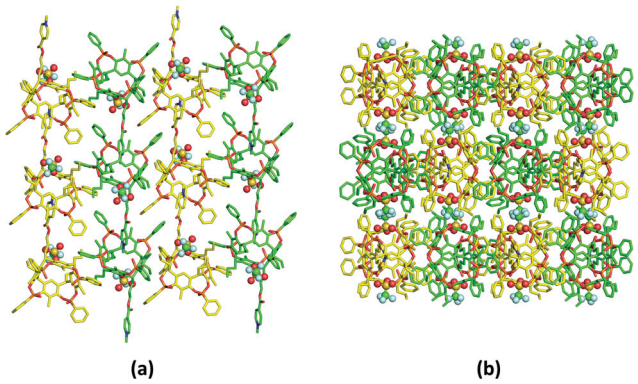

Fig. 1 Crystal packing of the **1CF$_3$SO$_3$** homopolymer as viewed (a) perpendicular to the linear polymeric chains and (b) along the polymeric chains. Chains with the dipolar moment pointing in opposite direction are shown in different colours. (Triflate ions are represented in ball and sticks.)

homopolymers by exploiting an integrated experimental approach based on PGSE (pulsed field gradient spin-echo),[32] NOE[33] and EXSY (exchange spectroscopy)[27] NMR experiments as well as cyclic voltammetry (CV), differential pulse voltammetry (DPV) and spectroelectrochemical measurements.

In detail, the supramolecular solution structures of ionic host–guest cavitands **1I**, **1CF$_3$SO$_3$** and **3I** and dimer **2·3PF$_6$** (Scheme 1) were investigated.

Supramolecular solution structure investigated by NOE measurements

The structure of supramolecular polymers in solution was investigated by using a combination of homo- and heteronuclear Overhauser NMR experiments. In the ^{1}H-NOESY NMR spectrum of **1CF$_3$SO$_3$** in $CDCl_3$ (Fig. 2), a strong contact was observed between **Ar-*Me*** and ***o*-PyMe** and a weak/medium one between **Py-*Me*** and **Ar-*H*** resonances. Both NOE interactions, not expected if the monomeric **1CF$_3$SO$_3$** would be the main species in solution, indicate close proximity between the pyridinium and phosphonate fragments, confirming formation of supramolecular adducts in solution. In particular, **MePy$^+$** moieties are located near the **P═O** groups: from this position the pyridine protons of one unit, being far away from their cavitand skeleton, can interact with the Ar protons of the cavitand skeleton belonging to another unit.

The anion–cation relative position in solution for the homopolymer **1CF$_3$SO$_3$** was determined by detecting dipolar interionic interactions in the ^{19}F,^{1}H-HOESY NMR spectrum at room temperature (Fig. 3). Normalization of the experimental cross peaks intensities, by taking into account the number of equivalent nuclei,[26] gives the results reported in Table 1. Strong contacts were observed between F-atoms of the counterion and aliphatic chain resonances and **Ar-H** resonances of the cavitand fragment. Very weak contacts were detected with **Ar-Me** and **Py-Me** resonances, whereas the anion did not show any interaction with protons of the phenyl ring bonded to the phosphorus. This pattern of heteronuclear Overhauser contacts, together with the trend of intensities reported in Table 1, indicates that the $CF_3SO_3^-$ is mainly located on the plane of the cavitand within the aliphatic chains, as shown in Fig. 3.

From this position, the anion has the possibility to weakly interact with Me-Py and the Ar-Me protons. This cation–anion

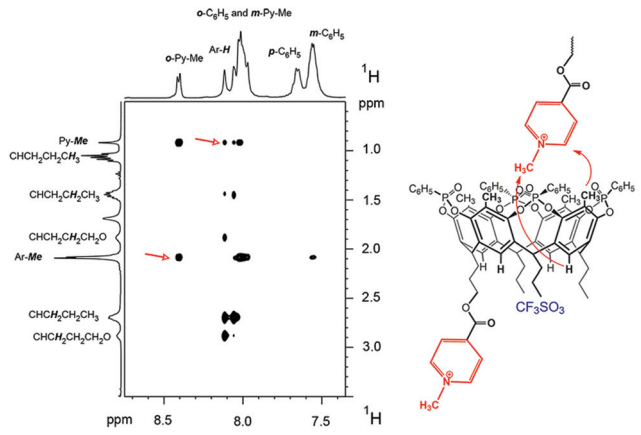

Fig. 2 A section of the ^{1}H-NOESY NMR spectrum (400.13 MHz, 296 K, $CDCl_3$) of **1CF$_3$SO$_3$** (22.3 mM).

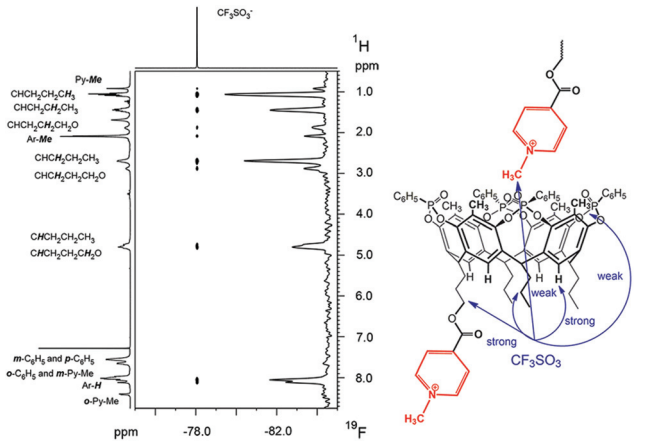

Fig. 3 ^{19}F,^{1}H-HOESY NMR spectrum (376.65 MHz, 296 K, $CDCl_3$) of complex **1CF$_3$SO$_3$** (22.3 mM). On the right, the column projection is reported.

Table 1 Relative heteronuclear Overhauser intensities determined by arbitrarily fixing at 1 the intensity of the NOE heteronuclear Overhauser contact between the anion resonances and Ar-*H* resonance

	1CF$_3$SO$_3$
Ar-H	1
$CHCH_2CH_2CH_3$ and $CHCH_2CH_2CH_2O$	0.62
$CHCH_2CH_2CH_2O$	0.49
$CHCH_2CH_2CH_3$	0.95
Ar-Me	0.12
$CHCH_2CH_2CH_2O$	0.28
$CHCH_2CH_2CH_3$	0.65
$CHCH_2CH_2CH_3$	0.99
Py-Me	0.08

relative position is the same observed in the solid-state structure of the homopolymer.[19]

The kinetic stability of polymers **1I**, *i.e.* the rate of formation and breaking of the supramolecular polymer, is an additional key aspect to take into account when describing their solution behaviour. Since solutions of **1I** display only one set of NMR resonances, such information cannot be easily derived. It can be, nevertheless, obtainable using a model solution system consisting of **3PF$_6$** and two equivalents of **2** (Scheme 1), exploiting the much lower tendency of **3PF$_6$** to form homopolymers.[19] Under these conditions, two well-separated ^{1}H NMR resonances are observed for the **Ar-Me** moiety of **2**, one related to **2·3PF$_6$** and the other to free **2**. Monitoring the chemical exchange between these two resonances by ^{1}H-EXSY NMR experiments allowed extracting the rate constant (k_{obs}) for the interconversion between free **2** and **2·3PF$_6$**. k_{obs} was found to be equal to 1.7 s^{-1}, 45 s^{-1} and 6.3 s^{-1} in $CDCl_3$ at 0.3 mM, in $CDCl_3$ at 2.1 mM and in $CDCl_3$/CD_3OD (92/8) at 0.3 mM, respectively. This indicates that formation/rupture of supramolecular polymers is accelerated by increasing concentrations of monomer whereas a slight increase of k_{obs} is observed when a small amount of CD_3OD is added.

Supramolecular solution structure obtained by PGSE NMR experiments

Additional information on the solution behaviour of the homopolymer **1I** can be obtained by PGSE diffusion NMR measurements which allow obtaining information on the average size of the supramolecular aggregates and, consequently, on the chemical origin of self-aggregation.[34] Initially, diffusion experiments were targeted for the homopolymer **1I** as a function of concentration in $CDCl_3$ (1.5 mM, 5.5 mM, 10.5 mM, 22.3 mM, 41.0 mM, 64.7 mM, 88.0 mM, and 147.0 mM). For such a series of measurements, we unexpectedly found that the standard plots of $\ln(I/I_0)$ *versus* G^2 showed sizable curvature at all investigated concentrations: average values of the diffusion coefficient (D_t) cannot be obtained by linear regression of experimental data and a different approach is necessary in order to obtain information on the self-aggregation tendency (see below). Linear trends are expected in the case of a single species or a monodisperse distribution of species in fast exchange in the PGSE NMR timescale (Δ). Nevertheless, ^{1}H-EXSY measurements indicate that exchange occurs on the same time-scale of diffusion, suggesting that **1I** is present in the form of a polydispersed distribution in slow exchange in the NMR timescale. This is reasonably due to the action of more than one type of self-assembly motif. The simplest hypothesis is to consider that formation of linear host–guest chains is coupled with further self-organization of the chains into bundles which are held together by inter-chain electrostatic interactions as observed in the solid state structure of **1CF$_3$SO$_3$** (Fig. 1). The PGSE methodological approach was tested by performing some measurements on diluted $CDCl_3$ solutions of the dimer **2·3PF$_6$**, the stopper **3I**, and on solutions of **1I** in $CDCl_3$/CD_3OD (92/8) solvent mixture. The results are reported in Table 2. In all cases, linear trends are observed and fitting according to eqn (3) allowed obtaining D_t values that were interpolated with eqn (14) (see the next sections), showing the dependence of D_i *vs. i.* The apparent number of monomers (i) in the supramolecular polymer as a function of concentration was obtained (Table 2). The values of i obtained (entries 5 and 6 in Table 2, for **2·3PF$_6$**, and entry 1 in Table 2, for **3I** at low concentration) are in good agreement with the predictions of eqn (13) (see next sections). PGSE measurements for **3I** at higher concentrations (entries 2–4 in Table 2) clearly indicate the formation of supramolecular aggregates of few units, since values of D_t obtained for these concentrations are lower than 4.66×10^{-10} m^2 s^{-1} (the theoretical value for the monomer), consistent with its low tendency to aggregate. Similarly to **3I** and differently from the behaviour in pure $CDCl_3$, plots of $\ln(I/I_0)$ *versus* G^2 are also linear for solutions of **1I** in $CDCl_3$/CD_3OD (92/8, entries 7–10, Table 2). It is reasonable to hypothesize that the presence of a minimal amount of CD_3OD in $CDCl_3$ tends to disfavour the additional self-organization of the chains into bundles, as will be further discussed below (cyclic voltammetry, differential pulse voltammetry and spectroelectrochemical measurements).

Table 2 Diffusion coefficients (D_t 10^{-10} m^2 s^{-1}) and number of monomer units *i*, for compounds **1I**, **3I** and dimer **2·3PF$_6$** as a function of concentration and solvent (*C*, mM)

Entry (Δ, ms)	Solvent	*C* (mM)	D_t	i
3I				
1 (120)	$CDCl_3$	0.2	3.80	1.8
2 (120)	$CDCl_3$	1.0	3.15	2.6
3 (120)	$CDCl_3$	11.0	2.41	4.2
4 (120)	$CDCl_3$	20.0	2.22	4.9
2·3PF$_6$				
5 (120)	$CDCl_3$	1.0	3.52	2.0
6 (120)	$CDCl_3$	3.0	3.40	2.2
1I				
7 (120)	$CDCl_3$/CD_3OD (92/8)	5.5	1.72	7.3
8 (120)	$CDCl_3$/CD_3OD (92/8)	13.4	1.33	10.8
9 (120)	$CDCl_3$/CD_3OD (92/8)	22.3	1.01	16.0
10 (120)	$CDCl_3$/CD_3OD (92/8)	41.4	0.72	25.5

As stated above, the non-linear trends of $\ln(I/I_0)$ *versus* G^2 plots, observed for **1I** in $CDCl_3$ at different concentrations, suggest the presence of a polydispersed distribution in slow exchange and require a different treatment of the experimental data. In the case of polydispersed distribution, the intensity of the PGSE signal depends on the diffusion coefficient of each species and on the concentration of the monomer responsible for the resonance signal and present in oligomers in solution, therefore:

$$I = \sum_i I_{0,i} \exp\left[-(\gamma\delta)^2 D_i \left(\Delta - \frac{\delta}{3}\right) G^2\right]. \quad (4)$$

Considering that the initial intensity of the signal, *i.e.* at field gradient value equal to zero, is proportional to the molar fraction of each polymeric species, multiplied by the number of monomers present in the polymer, eqn (4) can be written as:

$$I = I_0 \sum_i \frac{C_i \cdot i}{C_{tot}} \cdot \exp\left[-(\gamma\delta)^2 \left(\Delta - \frac{\delta}{3}\right) D_i G^2\right]. \quad (5)$$

In order to provide a fitting of experimental data using eqn (5), the values of the concentration of each polymeric species

(C_i) and the hydrodynamic translational diffusion coefficients (D_i) are required.

Distribution of polymeric species

Different models for the polymerization were evaluated, each of them corresponding to a different distribution of the polymeric species.

The first model, called the Sequential Equal K (SEK) model,[35] consists of a stepwise polymerization for which every subsequent step has the same constant, K_{SEK}, as the previous ones (isodesmic model).

The second model for the polymerization equilibrium that was taken into account is the Attenuated K (AK) model.[35] In this model, the thermodynamic constants for the formation of increasingly longer species decrease proportionally to $1/i$.

The results obtained with these two simple linear polymerization models, the X-ray structures, and the electrochemistry experiments suggested the possibility of a further aggregation process with formation of supramolecular bundles held together by dipolar, and quadrupolar interactions between antiparallel polymeric chains (see below). The SEK model was implemented with tetrameric aggregation equilibria having thermodynamic constants proportional to the number of monomers i of the linear polymer involved in the formation of antiparallel four-strain bundles (third model: SEK-TAi) or proportional to the fourth power of i (fourth model: SEK-TAi^4). These hypotheses are in line with the expected increase of dipolar energy contribution with the increase of the length of the polymer involved in the formation of supramolecular bundles.

In the linear polymerization process of the SEK model, the following chemical equations apply:

$$\begin{aligned} &A + A \overset{K_2}{\Leftrightarrow} A_2 && K_2 = K_{SEK} \\ &A_2 + A \overset{K_3}{\Leftrightarrow} A_3 && K_3 = K_{SEK} \\ &\cdots\cdots \\ &A_{i-1} + A \overset{K_i}{\Leftrightarrow} A_i && K_i = K_{SEK} \end{aligned}$$

where A is the monomer, while A_i is the oligomeric species formed by i monomers.

From these equilibrium equations, concentrations for the single polymeric species can be obtained depending on the free monomer concentration in solution, C_1 and SEK constant:

$$C_i = \frac{(C_1 K_{SEK})^i}{K_{SEK}} \tag{6}$$

For simplicity, we considered only the tetrameric aggregation of oligomeric species with the same number of monomers. Oligomeric species formed by i monomers are involved in the following equilibrium:

$$4A_i \overset{K_{TAi}}{\Leftrightarrow} (A_i)_4 \quad K_{TAi} = iK_{TA}$$

where the tetrameric aggregation constant is assumed proportional to the length of the polymeric chain in the SEK-TAi model.

From these equilibrium equations, concentration for the tetrameric species C_{i^4} can be obtained depending on the concentration of the polymeric chain with i monomers, C_i and the tetrameric aggregation constant, K_{TA}

$$C_{i^4} = C_{i^4} K_{TAi} = C_{i^4} iK_{TA}$$

From eqn (6) the concentration for the tetrameric species, C_{i^4}, can be expressed in terms of concentration of the free monomer in solution, C_1:

$$C_{i^4} = \frac{(C_1 K_{SEK})^{4i} iK_{TA}}{{K_{SEK}}^4} \tag{7}$$

The total concentration of the monomer C_t can be obtained as a sum of single oligomer concentrations multiplied by their length, i, plus the concentration of tetrameric species multiplied by the number of monomers in the aggregate, *i.e.* four times the length of a single chain:

$$\begin{aligned} C_t &= \sum_{i=1}^{\infty} iC_i + 4iC_{i^4} \\ &= \sum_{i=1}^{\infty} i\frac{(C_1 K_{SEK})^i}{K_{SEK}} + 4i\frac{(C_1 K_{SEK})^{4i} iK_{TA}}{{K_{SEK}}^4} \\ &= \frac{1}{K_{SEK}} \sum_{i=1}^{\infty} i(C_1 K_{SEK})^i + \frac{4K_{TA}}{{K_{SEK}}^4} \sum_{i=1}^{\infty} i^2 (C_1 K_{SEK})^{4i} \end{aligned}$$

both series converge under the condition $K_{SEK} \cdot C_1 < 1$ to:

$$C_t = \frac{C_1}{(1 - K_{SEK} C_1)^2} + \frac{4K_{TA}(K_{SEK} C_1)^4 [(K_{SEK} C_1)^4 + 1]}{{K_{SEK}}^4 [1 - (K_{SEK} C_1)^4]^3} \tag{8}$$

From eqn (8), the concentration of the free monomer in solution, C_1 can be evaluated knowing C_t, K_{SEK} and K_{TA} values. The distribution of all polymeric species in the SEK-TAi model is calculated using eqn (6) and (7).

For the fourth model, SEK-TAi^4, the tetrameric aggregation constant is assumed proportional to the fourth power of the number of monomers:

$$4A_i \overset{K_{TAi}}{\Leftrightarrow} (A_i)_4 \quad K_{TAi} = i^4 K_{TA4}$$

The distribution of the tetrameric species, C_{i^4} is

$$C_{i^4} = C_{i^4} i^4 K_{TA4}$$

and considering eqn (6):

$$C_{i^4} = \frac{(C_1 K_{SEK})^{4i} i^4 K_{TA4}}{{K_{SEK}}^4} \tag{9}$$

For the SEK-TAi^4 model, the total concentration of the monomer C_t can be obtained as:

$$\begin{aligned} C_t &= \sum_{i=1}^{\infty} iC_i + 4iC_{i^4} \\ &= \sum_{i=1}^{\infty} i\frac{(C_1 K_{SEK})^i}{K_{SEK}} + 4i\frac{(C_1 K_{SEK})^{4i} i^4 K_{TA4}}{{K_{SEK}}^4} \\ &= \frac{1}{K_{SEK}} \sum_{i=1}^{\infty} i(C_1 K_{SEK})^i + \frac{4K_{TA4}}{{K_{SEK}}^4} \sum_{i=1}^{\infty} i^5 (C_1 K_{SEK})^{4i} \end{aligned}$$

the series converge under the condition $K_{SEK} \cdot C_1 < 1$ to:

$$C_t = \frac{C_1}{(1-a)^2} + \frac{4K_{TA4}(a^{20} + 26a^{16} + 66a^{12} + 26a^8 + a^4)}{K_{SEK}{}^4(1-a^4)^6}$$

$$a = K_{SEK}C_1 \quad (10)$$

The concentration of the free monomer in solution, C_1 can be obtained from eqn (10) knowing C_t, K_{SEK} and K_{TA4} values. The distribution of all polymeric species in the SEK-TA*i*[4] model is calculated from eqn (6) and (9).

Distributions of polymeric species according to the SEK, AK, SEK-TA*i* and SEK-TA*i*[4] models were obtained using the software Octave[31] and *ad hoc* designed algorithms (see the ESI†).

Evaluation of the hydrodynamic translational diffusion coefficients based on the crystallographic structure

In order to obtain the hydrodynamic translational diffusion coefficients of the species in solution used in eqn (5), some hypothesis on D_i should be made. The X-ray crystallographic structure reported previously[19] (Fig. 1) shows the geometry of polymer formation and allows calculation of volumes and dimensions of oligomers. Using coordinates from the crystallographic 3D model and the software HYDRO,[36] we calculated D_i for the **1CF$_3$SO$_3$** monomer and for its oligomers. The structure of all the oligomers was assumed to be linear, similarly to that seen in the crystal.[19] Confirmation of the retention of this structure in solution comes from NOE and HOE techniques (*vide infra*). The tetraphosphonate cavitand can interpose between the methyl-pyridinium and the anion leading to the formation of the supramolecular linear polymer.

With HYDRO, the first 11 hydrodynamic translational diffusion coefficients, D_i, were calculated, for oligomers formed by up to 11 monomers. For a larger assembly, Perrin's law was applied to calculate the behaviour of D_i with $i > 11$.[37]

Considering the crystallographic structure, a prolate model can be used to approximate the polymer cylindrical shape and the axial ratio for the polymer with the polymerization degree of i, p_i, as:

$$p_i = \frac{a_{mono} \cdot i}{b} \quad (11)$$

where a_{mono} is the dimension of the monomer in the elongation direction and b is the dimension in the perpendicular direction. For each polymeric species, the Perrin S_i factor can be evaluated as:

$$S_i = 2\frac{\arctan h\xi_i}{\xi_i} \quad \text{with} \quad \xi_i = \frac{\sqrt{|p_i^2 - 1|}}{p_i} \quad (12)$$

Considering the monomer as an approximately spherical object, a_{mono} equals to b, p_1 equals to 1 and S_1 has the limit value of 2.

According to Perrin, Einstein and Stokes' equations, the hydrodynamic translational diffusion coefficient is expressed as:

$$D_i = \frac{k_B T}{6\pi\eta\sqrt[3]{\left(\frac{3V_i}{4\pi}\right)} \cdot \left(\frac{2\cdot\sqrt[3]{p_i^2}}{S_i}\right)} \quad (13)$$

The volume of the whole polymer can be considered as the volume of a cylinder with the height increasing with i. From eqn (13), the dependency of D_i from i can be written as

$$D_i = \frac{D_1 \cdot S_i}{2 \cdot \sqrt[3]{i \cdot p_i^2}} \quad (14)$$

The value of D_1 was optimized from the values of D_i calculated using HYDRO, with i from 2 to 11, applying the function *nlinfit* of the software Octave,[31] *i.e.* a nonlinear regression (see the ESI†).

Values calculated from Perrin's equations for the translational diffusion coefficients, D_i, were in good agreement with those obtained using the software HYDRO (Fig. S1†). With the same algorithm based on Perrin's equations, values of D_i were calculated for polymeric species up to i = 10 000.

Non-linear fitting of the PGSE data at different concentrations

Non-linear fittings of the PGSE data were performed using eqn (5), distributions calculated for different models and hydrodynamic translational diffusion coefficients, in order to obtain the thermodynamic constants for each model. In particular, the function *nlinfit* of Octave was used to fit the experimental data of the resonance intensity I, against the square of the field gradient G^2, varying the thermodynamic constants and the resonance intensity at $G = 0$ I_0, for 8 different total concentrations of the monomer, C_t (mM). Fig. 4 shows the fitting of two series of data, at concentrations 22.3 mM and 147 mM, respectively, considering a polymerization that follows the SEK model.

The fitting shows a good agreement for low monomer concentrations (Fig. 4a), but it gradually worsens increasing the monomer concentrations (Fig. 4b). Fig. S2 and S3† show the fitting of PGSE data at different concentrations according to the SEK model and Fig. S4† shows the polymeric distributions for each concentration, obtained using the K_{SEK} value optimized for each series of data (Table S1†).

This fitting procedure was also performed using the AK model. However, in this case the fitting is much worse than that obtained with the SEK model (see ESI, Fig. S5–S7†) for the higher monomer concentrations used in the experiments.

The values of K_{SEK} optimized against the PGSE data series are slightly different at different concentrations of monomers, as shown in Fig. 5. Values of K_{SEK} range from a minimum of 6.1×10^3 M^{-1} at low concentration of monomer to a maximum of 7.1×10^4 M^{-1}. This last value is in agreement with the K_a determined *via* ITC for **4** with methyl pyridinium (MePy$^+$) iodide in methanol (7.1×10^4 M^{-1}).[38] In particular, K_{SEK} values are fairly constant up to a monomer concentration of 20 mM and then begin to grow linearly. The values of the calculated average degree of polymerization obtained from distributions of polymeric species at low concentration of **1I** (Fig. 6) are in good agreement with the number of monomer units **i** obtained

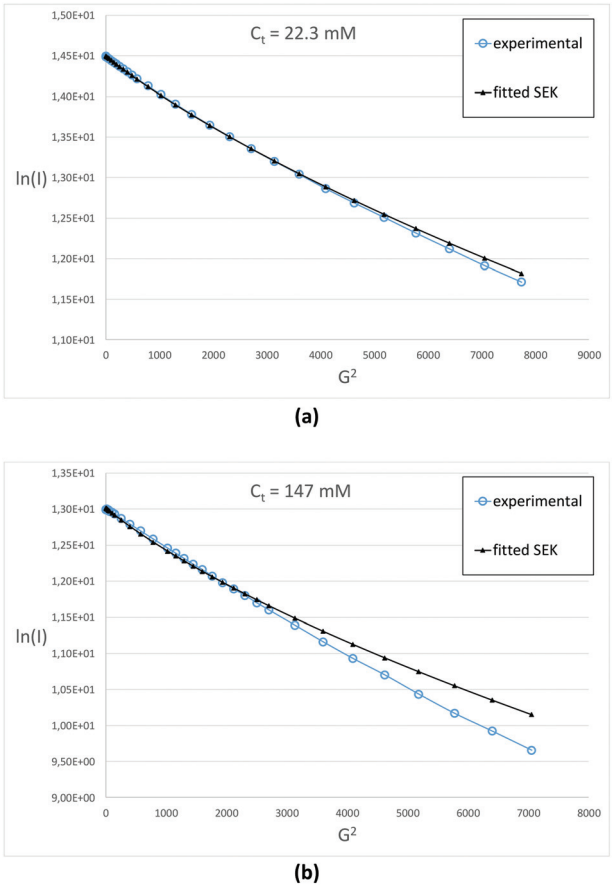

Fig. 4 Experimental (blue circles) and fitted (black triangles) data trend of ln(*I*) *versus* G^2 for **1I**. (a) At 22.3 mM in $CDCl_3$ (K_{SEK} = 1.18 × 10^4 M^{-1}); (b) at 147 mM in $CDCl_3$. (K_{SEK} = 7.15 × 10^4 M^{-1}.)

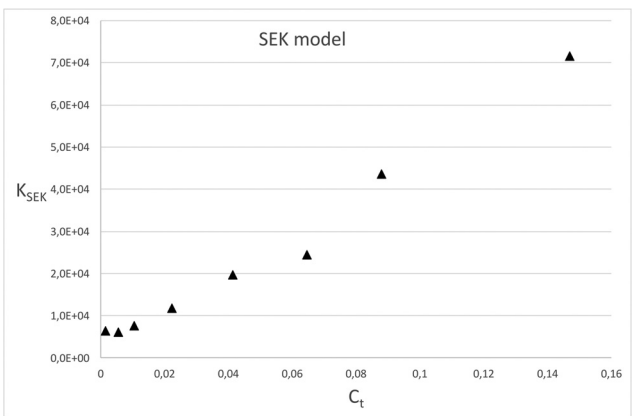

Fig. 5 Optimized values of K_{SEK} obtained for different monomer molar concentrations of **1I** in $CDCl_3$.

by linear fit of PGSE data collected in the presence of methanol (Table 2). These data suggest that at low concentration of monomer (and in the presence of methanol) the formation of linear supramolecular chains, as observed in the solid state, is the dominant self-aggregation process. This behaviour is con-

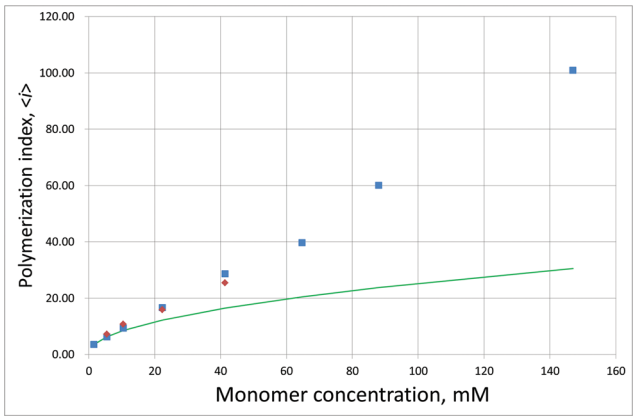

Fig. 6 Comparison between the calculated average degree of polymerization obtained from distributions of polymeric species with optimized SEK constants (blue cross) and the number of monomer units **i** obtained by linear fit of PGSE data collected in the presence of methanol (red cross). The full line represents the trend-line of the SEK model calculated with a minimum constant of 6.1 × 10^3 M^{-1}.

firmed by the SLS measurements.[19] Instead, when the concentration of the monomer is higher than 20 mM, other aggregation modes intervene, increasing the apparent value of K_{SEK} up to 10 times (Fig. 5). This additional aggregation mode is highlighted by the comparison between the values of the calculated average degree of polymerization obtained in the optimization of each series with respect to the trend-line calculated with the minimum K_{SEK} constant (6.10 × 10^3 M^{-1}) obtained at low concentration of **1I**, where aggregation processes should be negligible (Fig. 6). For the highest monomer concentration, namely 147 mM, the average degree of polymerization is 3.4 times higher than the trend-line (*i* = 103 and 30.5, respectively, Fig. 7).

A possible explanation for this behaviour is the formation of supramolecular bundles held together by dipolar and quadrupolar interactions between antiparallel polymeric chains, as observed in the solid state (Fig. 1).

The minimal aggregations in agreement with the apparent degree of polymerization (3.4 times higher than the trend-line, Fig. 6) are bundles composed of four antiparallel linear polymeric chains.

The antiparallel organization is suggested by the crystal packing, and the formation of supramolecular bundles is supported by electrochemical measurements (*vide infra*).

Two new models (SEK-TA*i* and SEK-TA*i*^{4}) were developed in order to take into account the formation of such "secondary" bundle-like structures in equilibrium with the non-aggregated polymer chains. Despite the oversimplification of the aggregation process present in these two new models, a significant improvement in the fitting of experimental PGSE data was observed in both cases (see ESI, Fig. S8–S10† for the SEK-TA*i* model and Fig. S11–S13† for the SEK-TA*i*^{4} model). The SEK-TA*i*^{4} model with the thermodynamic constant of tetrameric aggregation proportional to the fourth power of *i* reproduces better the experimental data than the SEK-TA*i* model

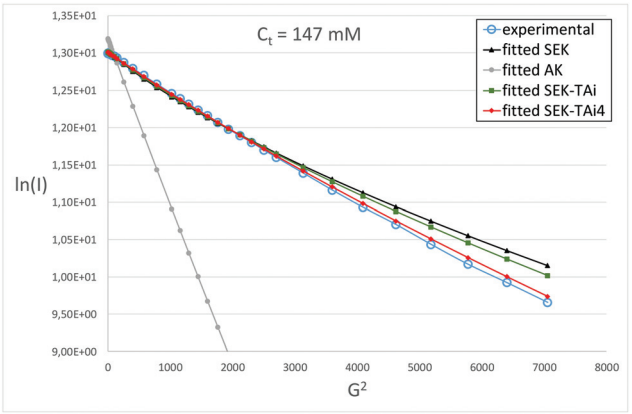

Fig. 7 Comparison between the fitting of PGSE experimental data (blue circles) obtained with four different models, *i.e.* SEK (black triangles), AK (grey circles), SEK-TA*i* (green squares) and SEK-TA*i*^{4} (red diamonds), for a monomer concentration of 147 mM.

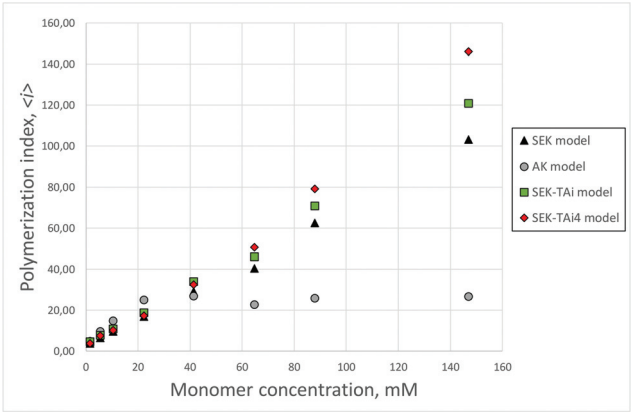

Fig. 9 Comparison between the calculated average degree of polymerization obtained from distributions of polymeric species in four different models, *i.e.* SEK (black triangles), AK (grey circles), SEK-TA*i* (green squares) and SEK-TA*i*^{4} (red diamonds).

with the K_{TAi} proportional to i, particularly at high concentration of the monomer (Fig. 7). The distribution of all polymeric species in the SEK-TA*i*^{4} model can be calculated from the K_{SEK} and K_{TA4} values. The speciation curves (Fig. 8) calculated with the K_{SEK} and K_{TA4} values obtained in the fitting procedure of the experimental PGSE measurements with a total monomer concentration C_t of 147 mM evidence the predominance of the aggregation process of the linear polymeric chains in bundles. The maximum concentration is calculated for a bundle of four linear chains each one formed by 31 monomeric units (Fig. 8). The comparison between the calculated average degree of polymerization obtained from distributions of polymeric species in four different models, *i.e.* SEK, AK, SEK-TA*i* and SEK-TA*i*^{4} at different concentrations of monomer is shown in Fig. 9. The SEK models implemented with a tetrameric aggregation process (SEK-TA*i* and SEK-TA*i*^{4}), which fit better the experimental PGSE data at higher monomer concentrations, show the calculated average degree of polymerization significantly higher with respect to the pure SEK model.

In particular, the SEK-TA*i*^{4} model, having the best fit of PGSE data (Fig. 7), shows a maximum value of the average degree of polymerization of 146 for a total monomer concentration of 147 mM. The corresponding value for the SEK-TA*i* model is 121 and 103 for the pure SEK model (Fig. 9).

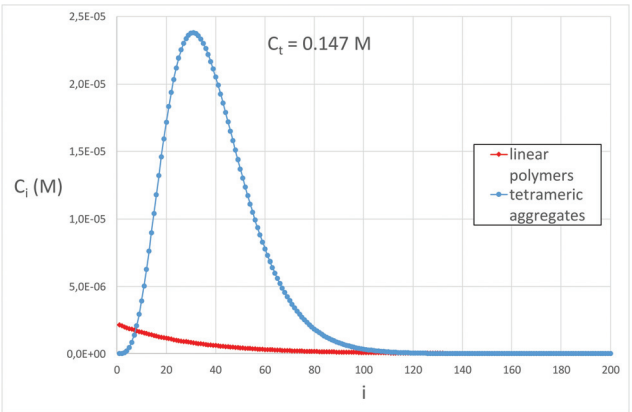

Fig. 8 Distribution of linear polymeric chain (red circles) and four chain bundle aggregates (blue circles) obtained using the SEK-TA*i*^{4} model, with K_{SEK} (4.55×10^5 M^{-1}) and K_{TA4} (6.13×10^{13} M^{-3}) values optimized to fit the experimental PGSE measurements for a monomer concentration of 147 mM.

Electrochemical properties

The electrochemical properties of the systems **1**$^+$, **3**$^+$, **4·3**$^+$ and **4·5**$^+$ were explored by means of cyclic voltammetry (CV), differential pulse voltammetry (DPV) and spectroelectrochemical measurements.

The aim of this study is to understand the electrochemical behaviour of the homopolymer **1I** on the basis of the results obtained from the investigation of the system **4·5** which constitutes a good model for the host–guest association that leads to supramolecular polymerization.[23] In fact, the results obtained in that case were promising about the possibility of controlling electrochemically the self-assembly of the supramolecular polymer.

The electroactive unit of the monomer **1** is the MePy$^+$ moiety, whose electrochemical behaviour is known both when it is free and complexed by the P=O groups of the tetraphosphonate cavitand (see system **4·5**). In order to obtain an even better model for the system **1I**, we performed electrochemical experiments on the thio-systems **3CF$_3$SO$_3$** and dimeric **4·3CF$_3$SO$_3$**.

Model systems

Cavitand **3** constitutes a good model for the study of the electrochemical properties of the MePy$^+$ unit of the monomer **1** when it is not complexed by the P=O groups in the polymeric structure.

This species exhibits a reversible reduction process at −0.69 V *vs.* SCE (Fig. S14†), clearly assigned to the first reduction of its MePy$^+$ unit by comparison with compound **5**. At potentials more negative than −1.2 V there are overlapping irreversible

Table 3 Electrochemical data for the two reduction processes of the $MePy^+$ unit in the investigated compounds (CH_2Cl_2/$TBAPF_6$, room temperature, glassy carbon electrode; ferrocene was used as an internal reference, $E(Fc^+/Fc)$ = +0.46 V *vs.* SCE)

System	E'/V *vs.* SCE	E''/V *vs.* SCE
3	−0.69[a]	[b]
4·3	−0.75[a]	[b]
5	−0.70[a]	−1.57[c]
4·5	−0.80[c]	−1.57[c]
1	−0.75[c], −1.19[c]	−1.50[c,d]

[a] Half wave potential values of reversible process. [b] The voltammetry signal for the MePy+ second reduction is covered by overlapping irreversible peaks ascribed to reduction of the P═S moieties of the cavitand. [c] Chemically irreversible process; potential value estimated from the DPV peak at a scan rate of 20 mV s^{-1}. [d] Strongly affected by electrode adsorption.

waves, most likely due to reduction of the P═S groups, which prevent the observation of the second reduction process of the methylpyridinium unit, expected at around −1.6 V. The DPV measurements confirm these observations.

The electrochemical behaviour of the complex **4·3** (Fig. S15†), which should reflect the properties of the $MePy^+$ unit of the monomer **1** when it is complexed by the P═O groups in the supramolecular polymer, is qualitatively similar to that of system **3**. The reversible wave at −0.75 V *vs.* SCE is assigned to the first monoelectronic reduction of the $MePy^+$ unit of **3**, which occurs at −0.69 V in the absence of the P═O cavitand. Such a negative shift can be interpreted in terms of the stabilization offered by the cavity of the P═O cavitand to the $MePy^+$ unit of **3**, in agreement with the results obtained for the **4·5** model system (Table 3).[23]

As observed for **3** alone, the second reduction process of the $MePy^+$ unit is hidden by intense irreversible waves at potentials more negative than −1.2 V, assigned to the reduction of the P═S cavitand moiety. Therefore, the voltammetry data yield no indication on the fate of the complex after monoelectronic reduction of **3**. On the basis of the strict similarity of this system with **4·5**, it is reasonable to expect that one-electron reduction of the $MePy^+$ unit leads to substantial disassembly of the complex.[23] The apparent reversibility of the CV wave shown in Fig. 11 indicates that the chemical rearrangements possibly associated with the electrochemical processes are fast on the cyclic voltammetry time scale.

Supramolecular polymer 1I

In the examined potential window, the self-assembling system **1I** undergoes three chemically irreversible reduction processes (Fig. 10). All of them have to be attributed to the $MePy^+$ unit, which is the sole electroactive unit of **1**. The reduction potentials obtained from the DPV peaks are −0.75 V, −1.19 V, and −1.50 V *vs.* SCE, respectively (Table 3).

In the CV, because of the chemical irreversibility of the processes, we consider the potential values of the cathodic peaks. The CV of the solution with [**1**] = 0.64 mM shows three cathodic peaks at −0.78 V, −1.22 V and −1.53 V *vs.* SCE, respectively.

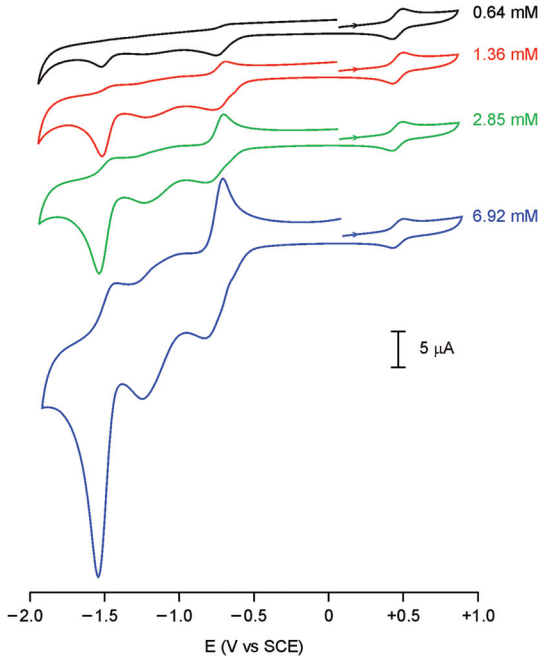

Fig. 10 Cyclic voltammograms for the reduction of the homopolymer **1I** at various monomer **1** concentrations (CH_2Cl_2 with 0.68 M $TBAPF_6$, glassy carbon electrode, scan rate 200 mV s^{-1}). The reversible wave at +0.46 V *vs.* SCE is that of ferrocene used as an internal standard.

The waves at −0.78 V and −1.53 V can be unambiguously attributed to the first and second reduction processes of the $MePy^+$ unit, respectively, by comparison with model systems. The first reduction wave occurs at a potential consistent with a $MePy^+$ unit encircled by the cavitand,[23] in agreement with the fact that under the conditions employed the vast majority of **1** species are self-assembled into polymeric aggregates **1I**.[19]

The reduction process responsible for the cathodic wave at −1.22 V cannot be straightforwardly assigned. To understand the origin of this process, we performed further CV studies upon changing the monomer concentration (Fig. 10) and the potential scan rate (Fig. 11).

Upon increasing the concentration of **1**, it can be noticed that the peak at −1.22 V grows in intensity at the expense of the peak at −0.78 V (Fig. 10) which, at the same time, improves its chemical reversibility (see the anodic wave at *ca.* −0.70 V). The same qualitative changes in the CV pattern – *i.e.*, the relative increase of the peak at −1.22 V compared with that at −0.78 V and the enhancement of the chemical reversibility of the first reduction process – are observed on increasing the potential scan rate (Fig. 11). This picture can be interpreted considering that the polymer chains **1I** can associate together side-by-side to generate bundles stabilized by a combination of multipole interactions and van der Waals forces. In solution, such bundle-like structures are in equilibrium with the non-aggregated polymer chains. Because the cationic pyridinium units along the chains are strongly involved in the multipole interactions responsible for the formation of the bundles, it can be expected that the $MePy^+$ moieties belonging to polymer

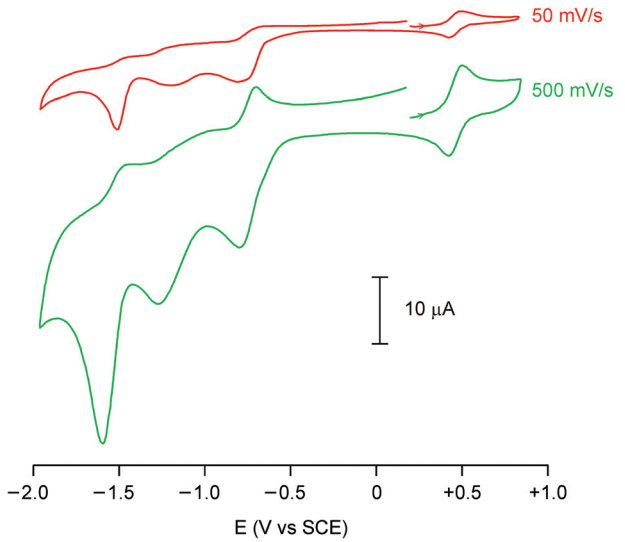

Fig. 11 Cyclic voltammograms for the reduction of homopolymer **1I** at different scan rates (monomer concentration 5.04 mM, CH_2Cl_2 with 0.51 M $TBAPF_6$, glassy carbon electrode). The reversible wave at +0.46 V *vs.* SCE is that of ferrocene used as an internal standard.

chains associated in a bundle are stabilized, and hence become more difficult to reduce, compared to units belonging to non-aggregated polymer chains.

Therefore, while the process at −0.78 V is assigned to cavitand-complexed $MePy^+$ units in non-aggregated chains, the one at −1.22 V is attributed to cavitand-complexed $MePy^+$ units in bundled chains (Scheme 2).

Such an interpretation is fully consistent with the observed CV behaviour. The intensity ratio of the peaks assigned to reduction of bundles and single chains is expected to increase at higher monomer concentrations, when the equilibrium is displaced towards the formation of the bundles. This is exactly what is observed in the experiments (Fig. 10). Because there is a chemical equilibrium between bundled and unbundled polymer chains, the reduction of the $MePy^+$ units in the non-associated chains at −0.78 V is expected to shift the equilibrium away from the bundled structure towards the unbundled one. In fact, upon increasing the potential scan rate, the cathodic peak at −1.22 V is enhanced (Fig. 11) because the disruption of the bundles in consequence of the first reduction (−0.78 V) becomes slow in the time scale of the electrochemical experiment. Conversely, the equilibrium shift leading to a decrease of the concentration of the bundles (and hence of the corresponding current intensity at −1.22 V) can be observed at slower scan rates (Fig. 11).

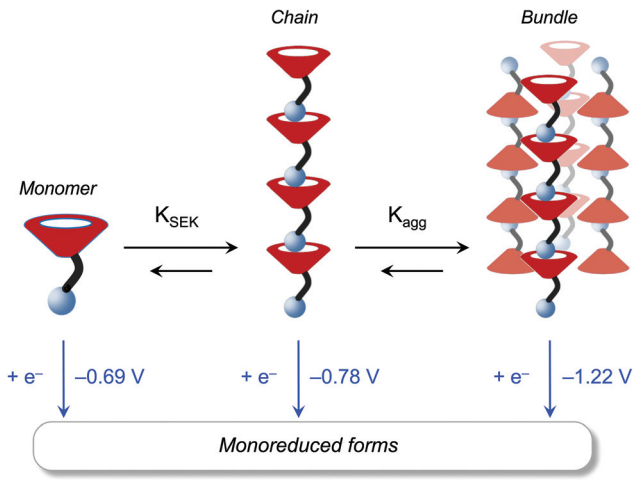

Scheme 2 Representation of the self-assembly processes of polymer chains **1I** and bundle aggregates $(\mathbf{1I})_n$ from monomer **1**, and associated electrochemical one-electron reduction of their $MePy^+$ units. The potential value for the reduction of the $MePy^+$ unit in model compound **3** is taken as the reduction potential of monomeric **1**.

At this point, it should be assessed whether the first reduction of the $MePy^+$ unit of **1** leads to the disassembly of the polymer, as it happens for the **4·5** model system. In the case of **1I**, however, the potential for the second reduction process of the $MePy^+$ unit does not give a clear indication about the fate of the aggregate after the first reduction. To this aim, we performed spectroelectrochemical measurements on cavitand **3** and polymer **1I**.

The absorption spectrum of the monoreduced **3** species, obtained upon electrolysis of **3** at −1.0 V *vs.* an Ag pseudo-reference electrode, shows two intense bands with λ_{max} = 304 and 395 nm (Fig. 12a) that are characteristic of the monoreduced MePy unit. The absorption spectrum obtained upon electrolysis of a solution of polymer **1I** at −1.33 V *vs.* an Ag pseudo-reference electrode (Fig. 12b) shows the same bands observed for the monoreduced **3** species. If the monoreduced MePy moiety remained included in the cavitand, it is reasonable to assume that the absorption spectrum of the former would be affected in some way. Hence, the spectroelectrochemical results suggest that the polymer is disassembled upon one-electron reduction of the $MePy^+$ moiety.

The CV cathodic wave at −1.53 V, assigned to the second reduction of the $MePy^+$ units, is strongly affected by electrode adsorption phenomena for scan rates higher than 50 mV s^{-1}. Such a behaviour suggests that under these conditions the monoreduced species precipitate onto the electrode surface. The potential for this process, however, can be reasonably estimated at a slow scan rate (20 mV s^{-1}) by DPV measurements (Table 3). It is interesting to note that the process takes place at a less negative potential (−1.50 V) compared to the same process in a free $MePy^+$ (−1.57 V). This observation might indicate that the **1** species, which become non-associated in their neutral form (*i.e.* after one-electron reduction of their $MePy^+$ units, *vide supra*), self-assemble again in their negatively charged form (*i.e.* upon two-electron reduction). The stability of the resulting aggregate would account for the fact that the second reduction of **1** is easier than that of model compound **5**, leading to a positive shift in the corresponding redox potential.

Our data are insufficient to allow speculations about the nature of these aggregates, but their formation cannot be simply explained in terms of host–guest interactions between a doubly reduced MePy moiety and a P═O cavitand, because the **4·5** model system shows a different behaviour.

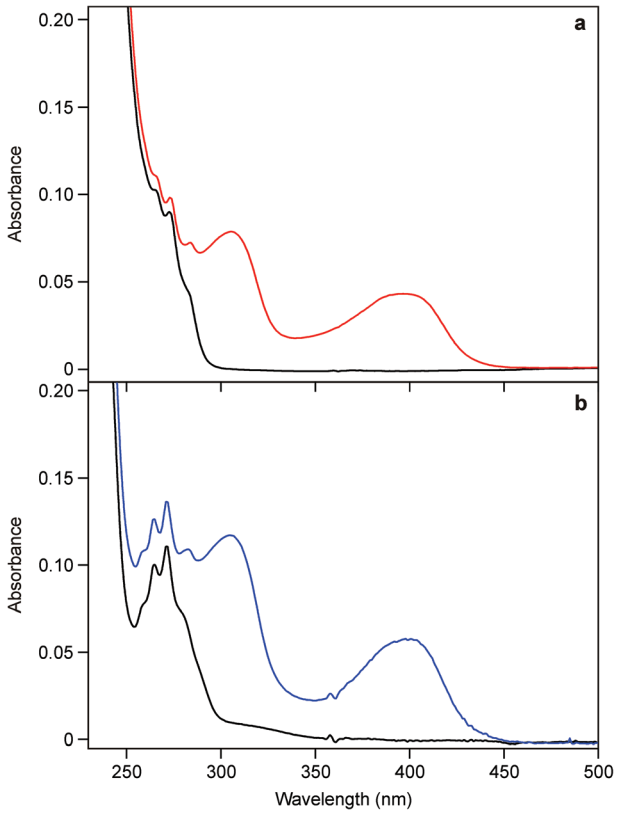

Fig. 12 (a) Absorption spectrum of **3** before (black line) and after (red line) exhaustive electrolysis at −1.0 V. Conditions: 0.839 mM, CH_2Cl_2/86.0 mM $TBAPF_6$. (b) Absorption spectrum of the supramolecular polymer **1I** before (black line) and after (blue line) exhaustive electrolysis at −1.33 V. Conditions: Monomer concentration 0.706 mM, CH_2Cl_2/73.4 mM $TBAPF_6$. Platinum grid working electrode, Ag pseudo-reference electrode, and optical path length 180 μm.

In summary, the self-assembly equilibrium leading to the formation of the supramolecular polymer **1I** can be controlled electrochemically (Scheme 2); specifically, one-electron reduction of the $MePy^+$ unit of **1** causes the disassembly of the polymer. The reversibility of the switching process, however, is limited by the poor chemical reversibility of the $MePy^+$ reduction. In addition, voltammetry measurements suggest that the polymer chains **1I** undergo aggregation, in line with the NMR results.

Conclusions

The overall picture emerging from the NMR and voltammetry experiments supported by theoretical models shows that: (i) below 20 mM monomer concentration, the main aggregation process is the isodesmic linear polymerization of cavitand **1** and (ii) above 20 mM, dipolar and quadrupolar interactions involving longer linear chains become energetically relevant. At high monomer concentration (147 mM) tetrameric bundles, formed by the antiparallel aggregation of four linear chains, prevail, as inferred by the non-linear fitting of the PGSE data obtained using the SEK-TA*i*[4] model (Fig. S13†). Interestingly, the bundle assembly results in a ten-fold increase of K_{SEK}, showing a synergistic effect on the aggregation process between linear polymerization and bundle assembly. Furthermore, the bundle formation increases the stability of the linear chains toward electrochemical reduction. The different nature of the weak interactions of the two assembly modes allowed devising two orthogonal disassembly procedures. The dipolar and quadrupolar interactions leading to bundle aggregation are more sensitive to solvent polarity than the host–guest interactions. On the other hand, bundles are more stable than linear chains toward electrochemical reduction. Tuning either one of the two stimuli allows controlling the equilibrium toward the desired species.

Author contributions

Daniele Zuccaccia: formal analysis and investigation; Roberta Pinalli: resources, investigation, and writing – review and editing; Rita De Zorzi: investigation; Monica Semeraro: investigation; Alberto Credi: conceptualization, project administration, and writing – original draft; writing – review and editing; Cristiano Zuccaccia: investigation; Alceo Macchioni: project administration, writing – original draft; writing – review and editing; Silvano Geremia: conceptualization, formal analysis, project administration, writing – original draft; writing – review and editing; Enrico Dalcanale: conceptualization, supervision, writing – original draft; project administration, writing – review and editing.

Conflicts of interest

There are no conflicts to declare.

Acknowledgements

Financial support from the Italian Ministry of University and Research (PRIN 2017 projects 20179BJNA2 and 20173L7W8K), and the European Union (H2020 FET-OPEN “Magnify” no. 801378) is gratefully acknowledged.

This work has benefited from the equipment and framework of the COMP-HUB Initiative of the University of Parma and AMIS from the University of Udine, funded by the ‘Departments of Excellence’ program of the Italian Ministry for Education, University and Research (MIUR, 2018-2022).

Notes and references

1 N. Roy, B. Bruchmann and J.-M. Lehn, *Chem. Soc. Rev.*, 2015, **44**, 3786.
2 Y. Zhang and M. Barboiu, *Chem. Rev.*, 2016, **116**, 809.
3 T. Aida, E. W. Meijer and S. I. Stupp, *Science*, 2012, **335**, 813.

4 O. J. G. M. Goor, S. I. S. Hendrikse, P. Y. W. Dankers and E. W. Meijer, *Chem. Soc. Rev.*, 2017, **46**, 6621.
5 M. J. Webber, E. A. Appel, E. W. Meijer and R. Langer, *Nat. Mater.*, 2015, **15**, 13.
6 Y. Lu, A. A. Aimetti, R. Langer and Z. Gu, *Nat. Rev. Mater.*, 2016, **2**, 16075.
7 (*a*) H. Ouchi, T. Kizaki, M. Yamato, X. Lin, N. Hoshi, F. Silly, T. Kajitani, T. Fukushima, K.-I. Nakayama and S. Yagai, *Chem. Sci.*, 2018, **9**, 3638; (*b*) E. Moulin, J. J. Armao IV and N. Giuseppone, *Acc. Chem. Res.*, 2019, **52**, 975.
8 C. Fouquey, J.-M. Lehn and A.-M. Levelut, *Adv. Mater.*, 1990, **2**, 254.
9 V. Balzani, S. Campagna, G. Denti, A. Juris, S. Serroni and M. Venturi, *Acc. Chem. Res.*, 1998, **31**, 26.
10 S.-L. Li, T. Xiao, C. Lin and L. Wang, *Chem. Soc. Rev.*, 2012, **41**, 5950.
11 A. Harada, Y. Takashima and M. Nakahata, *Acc. Chem. Res.*, 2014, **47**, 2128.
12 J. Liu, C. S. Y. Tan, Y. Lan and O. A. Scherman, *Chem. Phys.*, 2016, **217**, 319.
13 H. Li, Y. Yang, F. Xu, T. Liang, H. Wen and W. Tian, *Chem. Commun.*, 2019, **55**, 271.
14 (*a*) T. Haino, Y. Matsumoto and Y. Fukazawa, *J. Am. Chem. Soc.*, 2005, **127**, 8936; (*b*) C. Capici, Y. Cohen, A. D'Urso, G. Gattuso, A. Notti, A. Pappalardo, S. Pappalardo, M. F. Parisi, R. Purrello, S. Slovak and V. Villari, *Angew. Chem., Int. Ed.*, 2011, **50**, 11956.
15 D.-S. Guo and Y. Liu, *Chem. Soc. Rev.*, 2012, **41**, 5907.
16 F. Tancini and E. Dalcanale, Polymerization with Ditopic Cavitand Monomers, in *Supramolecular Polymer Chemistry*, ed. A. Harada, Wiley-VCH Verlag Gmbh & Co. KGaA, Weinheim, Germany, 2012, pp. 71–93.
17 L. Pirondini, A. G. Stendardo, S. Geremia, M. Campagnolo, P. Samorì, J. P. Rabe, R. Fokkens and E. Dalcanale, *Angew. Chem., Int. Ed.*, 2003, **42**, 1384.
18 N. Nitta, M. Takatsuka, S. Kihara, T. Hirao and T. Haino, *Angew. Chem. Int. Ed.*, 2020, **59**, 16690.
19 R. M. Yebeutchou, F. Tancini, N. Demitri, S. Geremia, R. Mendichi and E. Dalcanale, *Angew. Chem., Int. Ed.*, 2008, **47**, 4504.
20 F. Tancini, R. M. Yebeutchou, L. Pirondini, R. Dezorzi, S. Geremia, O. A. Scherman and E. Dalcanale, *Chem. – Eur. J.*, 2010, **16**, 14313.
21 M. Dionisio, L. Ricci, G. Pecchini, D. Masseroni, G. Ruggeri, L. Cristofolini, E. Rampazzo and E. Dalcanale, *Macromolecules*, 2014, **47**, 632.
22 D. Masseroni, E. Rampazzo, F. Rastrelli, D. Orsi, L. Ricci, G. Ruggeri and E. Dalcanale, *RSC Adv.*, 2015, **5**, 11334.
23 B. Gadenne, M. Semeraro, R. M. Yebeutchou, F. Tancini, L. Pirondini, E. Dalcanale and A. Credi, *Chem. – Eur. J.*, 2008, **14**, 8964.
24 J. Jeener, B. H. Meier, P. Bachmann and R. R. Ernst, *J. Chem. Phys.*, 1979, **71**, 4546.
25 R. Wagner and S. Berger, *J. Magn. Reson., Ser. A*, 1996, **123**, 119.
26 (*a*) B. Lix, F. D. Sönnichsen and B. D. Sykes, *J. Magn. Reson., Ser. A*, 1996, **121**, 83; (*b*) E. Menozzi, M. Busi, C. Messera, F. Ugozzoli, D. Zuccaccia, A. Macchioni and E. Dalcanale, *J. Org. Chem.*, 2006, **71**, 2617.
27 (*a*) C. L. Perrin and T. J. Dwyer, *Chem. Rev.*, 1990, **90**, 935; (*b*) D. Zuccaccia, L. Pirondini, R. Pinalli, E. Dalcanale and A. Macchioni, *J. Am. Chem. Soc.*, 2005, **127**, 7025.
28 (*a*) D. Zuccaccia and A. Macchioni, *Organometallics*, 2005, **24**, 3476; (*b*) A. Macchioni, G. Ciancaleoni, C. Zuccaccia and D. Zuccaccia, *Chem. Soc. Rev.*, 2008, **37**, 479; (*c*) P. S. Pregosin, P. G. A. Kumar and I. Fernández, *Chem. Rev.*, 2005, **105**, 2977.
29 R. Schlögl, H. J. Tyrell and K. R. Harris, *Ber. Bunsen-Ges. Phys. Chem.*, 1985, **89**, 209.
30 R. Mills, *J. Phys. Chem.*, 1973, **77**, 685.
31 J. W. Eaton, *J. Process Control*, 2012, **22**, 1433.
32 (*a*) Y. Cohen and S. Slovak, *Org. Chem. Front.*, 2019, **6**, 1705; (*b*) F. Zaccaria, C. Zuccaccia, R. Cipullo and A. Macchioni, *Chem. – Eur. J.*, 2019, **25**, 9930; (*c*) Y. Cohen, L. Avram, T. Evan-Salem, S. Slovak, N. Shemesh and L. Frish, in *Analytical Methods in Supramolecular Chemistry*, ed. C. A. Schalley, Wiley-VCH, Berlin, 2nd edn, 2012, vol. 1, ch. 7, pp. 197–286; (*d*) P. Stilbs, *Prog. Nucl. Magn. Reson. Spectrosc.*, 1987, **17**, 1–45; (*e*) Y. Cohen, L. Avram and L. Frish, *Angew. Chem., Int. Ed.*, 2005, **44**, 520.
33 (*a*) A. Macchioni, *Eur. J. Inorg. Chem.*, 2003, 195; (*b*) A. Macchioni, A. Magistrato, I. Orabona, F. Ruffo, U. Rothlisberger and C. Zuccaccia, *New J. Chem.*, 2003, **27**, 455; (*c*) L. Biasiolo, G. Ciancaleoni, L. Belpassi, G. Bistoni, A. Macchioni, F. Tarantelli and D. Zuccaccia, *Catal. Sci. Technol.*, 2015, **5**, 1558.
34 G. Bellachioma, G. Ciancaleoni, A. Macchioni, C. Zuccaccia and D. Zuccaccia, *Coord. Chem. Rev.*, 2008, **252**, 2224.
35 (*a*) F. Garland and S. D. Christian, *J. Phys. Chem.*, 1975, **79**, 1247; (*b*) R. B. Martin, *Chem. Rev.*, 1996, **96**, 3043; (*c*) L. Rocchigiani, G. Bellachioma, G. Ciancaleoni, S. Crocchianti, A. Lagana, C. Zuccaccia, D. Zuccaccia and A. Macchioni, *ChemPhysChem*, 2010, **11**, 3243.
36 J. Garcia de la Torre, S. Navarro, M. C. Lopez Martinez, F. G. Diaz and J. J. Lopez Cascales, *Biophys. J.*, 1994, **67**, 530.
37 F. Perrin, *J. Phys. Radium*, 1934, **5**, 497.
38 D. Menozzi, E. Biavardi, C. Massera, F.-P. Schmidtchen, A. Cornia and E. Dalcanale, *Supramol. Chem.*, 2010, **22**, 768.